



Anticorrosion Behaviour of a Hydrazone Derivative on 6061 Al-15%_(v) SiC_(P) Composite in Acid Medium: Experimental and Theoretical Calculations

Dhanya Shetty¹ · P. Preethi Kumari¹ · Suma A. Rao¹ · Prakash Shetty¹

Received: 17 December 2019 / Revised: 12 March 2020 / Accepted: 23 March 2020 / Published online: 6 April 2020
© Springer Nature Switzerland AG 2020

Abstract

The present work describes the evaluation of anticorrosion property of 4-hydroxy-*N'*-[3-phenylprop-2-en-1-ylidene] benzohydrazide (HBH) on 6061 Al-15%_(v) SiC_(P) composite (Al-CM) in 0.5 M hydrochloric acid medium. The results of electrochemical measurement and specimen morphology study are discussed in this work. The adsorption of HBH over the Al-CM surface is through physisorption and obeys the Langmuir's isotherm model. Potentiodynamic polarization study showed that the HBH acted as mixed inhibitor. The electrochemical impedance spectroscopy (EIS) study showed that the increase in the adsorption tendency of HBH on to the metal surface is due to increase in the polarization resistance. Density functional theory (DFT)-based calculations were carried out for both neutral and protonated HBH molecules which is well supported by the experimental observations.

Keywords Hydrazone · Acid corrosion · Impedance · Physisorption · Polarization

Abbreviations

Al-CM	6061 Al-15%(v) SiC(P) composite
HBH	4-Hydroxy- <i>N'</i> -[3-phenylprop-2-en-1-ylidene] benzohydrazide
HCl	Hydrochloric acid medium
EIS	Electrochemical impedance spectroscopy
PDP	Potentiodynamic polarization
OCP	Open-circuit potential
E_{corr}	Corrosion potential
%IE	Percentage Inhibition efficiency
CR	Corrosion rate
i_{corr}	Corrosion current density
DFT	Density functional theory
SEM	Scanning electron microscope
EDX	Energy-dispersive X-ray
AFM	Atomic force microscope

1 Introduction

The pertinent problems faced by many industries are corrosion of metals and material conservation. As the material comes in contact with corrosive environment, it leads to its destruction [1, 2]. Al and Al alloys are widely used in industries that show high corrosion resistance due to the passive film on their surface [3, 4]. However, their applications are limited due to their lower strength and stiffness. In order to enhance its strength and to provide better performance the requirement of such alloy is to reinforce with particles such as SiC. Aluminium alloy reinforced with SiC particles possess high-specific strength and hence find various applications in automobile, aviation, and military applications [5, 6]. The addition of SiC can cause discontinuities in the protective oxide film. This can lead to increase in the number of sites, where corrosion can occur and make the composite more vulnerable. The depletion of naturally occurring oxide layer takes place with reinforcement of SiC particulates which in turn accelerates the corrosion in corrosive environment [7, 8] Micro-galvanic corrosion of Al-CM is more likely to occur during acid pickling and descaling procedures used in the surface preparation of such composite material. The ceramic particles function as efficient cathodic sites and trigger corrosion in the presence of corrosive liquids [9, 10]. To overcome such problem, the use of inhibitor is

✉ P. Preethi Kumari
preethi.prabhu@manipal.edu

¹ Department of Chemistry, Manipal Institute of Technology, Manipal Academy of Higher Education, Manipal 576104, India

considered as the most practical method. The organic compounds containing hetero atoms, unsaturated bonds, aromatic rings showed very good inhibition efficiency against acid corrosion of Al-CM [11–13]. The literature study reveals the excellent corrosion inhibition tendency of some of the hydrazides, its derivatives and hydrazides containing imine group particularly on mild steel in different acid media [14–16]. The inhibitive nature of these compounds is accredited to their molecular structure. The unshared pair of electrons on the atoms such as N, O, S etc., π electrons, electron donating groups and planarity of the inhibitor molecule determines the film formation or adsorption of these molecules on the metallic surface. Despite its exceptional corrosion inhibition ability, only few hydrazides are used as inhibitor for Al and Al-based alloys and composites [17]. Hence, the purpose of the present work was to synthesize a hydrazide derivative, namely 4-hydroxy-*N'*-[3-phenylprop-2-en-1-ylidene] benzohydrazide (HBH) and to study its corrosion inhibition behaviour on Al-CM in 0.5 M hydrochloric acid medium at different temperatures by adopting electrochemical techniques. This study also includes the determination of activation, thermodynamic parameters and surface characterization using different techniques. Further theoretical calculations were done using DFT which is in agreement with the experimental results.

2 Experimental Details

2.1 Material

The present study makes use of 6061 Al-15%_(V) SiC_(P) composite (Al-CM) material as test specimen with composition depicted in Table 1. Cylindrical shaped test coupons of Al-CM material were mounted using cold setting resin. The flat specimen surface having exposed surface area of 1 cm² of the mounted part was then abraded using polishing papers

of different grades followed by disc polishing using levigated alumina abrasive as per standard metallographic practice.

2.2 Preparation of Medium

The medium used was standard hydrochloric acid solution. A stock solution of hydrochloric acid (1 M) was prepared by diluting a known volume of 37% AR grade hydrochloric acid to an appropriate volume to get required strength and standardized by volumetric method.

2.3 Preparation of HBH

An equimolar mixture of trans-3-Phenyl-2-propenal (0.01 mol) and 4-hydroxy benzohydrazide (0.01 mol) was dissolved in ethanol. The product formed after refluxing the reaction mixture for about 3 h. Ethanol was used for recrystallization of the product obtained after the filtration of reaction mixture. The synthetic route for the preparation of HBH is represented by Scheme 1.

2.4 Electrochemical Techniques

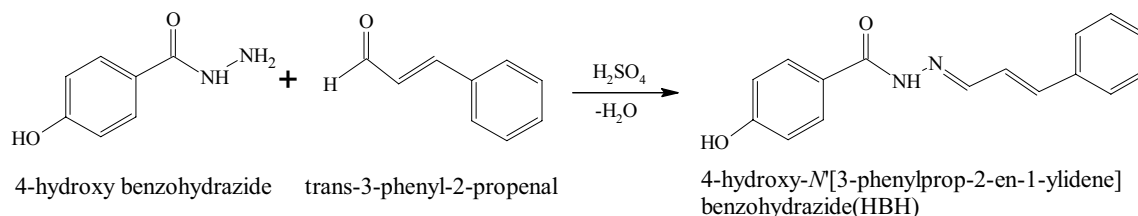
An electrochemical work station (CH Instrument USA Model 604D series with beta version software) along with conventional three electrode cell was used to perform the electrochemical techniques. The cell constitutes of a platinum and calomel electrode as counter and reference electrode, respectively. Freshly polished working Al-CM specimen was exposed to 0.5 M HCl within a temperature range of 303 to 323 K. The open circuit potential (OCP) is observed at the end of 30 min and recorded. The specimen was then polarised from -250 mV cathodic to +250 mV anodic with respect to OCP fixing a scan rate of 1 mV s⁻¹, the Tafel curves were recorded. In case of EIS a small amplitude of ac signal of 10 mV was applied to the system in the frequency range (10 kHz to 0.01 Hz) with respect to OCP and the Nyquist plot was recorded.

2.5 Quantum Chemical Study

The DFT calculations were done using Gaussian maestro material science software with the correlation factor

Table 1 Chemical composition of Al-CM material

Elements	Cr	Cu	Mg	Si	Al
Composition (wt%)	0.01	0.02	0.61	1.00	Balance



Scheme 1 Synthetic route for HBH

(B3LYP) and 631 + G as basis set [18]. The energies of the highest occupied (E_{HOMO}) and lowest unoccupied (E_{LUMO}) molecular orbitals were evaluated and which are then used to calculate other quantum chemical considerations. [19, 20].

2.6 Surface Morphological Studies

Surface morphological study was done using scanning electron microscope (SEM) and surface roughness of Al-CM specimen was determined by atomic force microscope (AFM). Chemical analysis of the specimen surface was done using energy-disperse X-ray (EDX).

3 Results and Discussion

3.1 IR Characterization Results of HBH

Crystalline white solid (95%); $\text{C}_{16}\text{H}_{14}\text{N}_2\text{O}_2$; m.p: 264–266 °C; IR (KBr) [cm^{-1}]: 3502 (OH *str.*), 3201 (NH *str.*), 3016 (Ar. CH *str.*), 1612 (C=O *str.*), 1558 (C=N *str.*), 1504 (Ar. C=C *str.*). ^1H NMR (400 MHz, DMSO- d_6) δ (ppm): 11.53 (1H, OH), 10.13 (1H, NH), 8.22 (1H, CH=N), 7.81–6.83 (9H, Ar. H), 2.15 (1H, CH). Figure 1a and b represents the IR and ^1H NMR spectrum of HBH molecule.

3.2 Potentiodynamic Polarization (PDP) Measurements

The PDP plots for the dissolution of Al-CM in presence of uninhibited and inhibited solution are shown in Fig. 2. The anodic potential is displaced in a positive direction by anodic polarization and cathodic potential is displaced in a negative direction by cathodic polarization. The point of intersection between the two rectilinear polarization curves in the PDP plots gives corrosion current density (i_{corr}), corrosion potential (E_{corr}). The experimental results obtained for corrosion of Al-CM without and with HBH are tabulated in Table 2.

The added inhibitor molecules get adsorbed over the Al-CM surface and hence reduce the corrosion rate. Generally, the presence of reinforcing element (SiC) enhances the corrosion rate of aluminum composite compared to aluminum-based alloys. Since the electrode potential of Si (−0.14 V) is more than the electrode potential of Al (−1.67 V), SiC will act as cathode-making Al as anode which results in galvanic corrosion leading to disintegration of aluminum matrix. The heterogeneous nature of the composite material due to the presence of SiC, increases the availability of the active sites for the adsorption of inhibitor molecules [21].

The inhibitor can be distinctively considered as anodic or cathodic type if the displacement in the E_{corr} exceeds ± 85 mV in the presence of inhibitor with respect

to that of uninhibited solution [22]. However, it is evident from the above Tafel plot that the corrosion potential does not show much variation in the presence of HBH in comparison with uninhibited solution. This shows that HBH acts as mixed type inhibitor by retarding both anodic and cathodic reactions. From the obtained i_{corr} values corrosion rate (CR) and percentage inhibition efficiency (% IE) were calculated using Eqs. (1) and (2), respectively.

$$\text{CR} (\text{mm y}^{-1}) = \frac{3270 \times EW \times i_{\text{corr}}}{d} \quad (1)$$

where, i_{corr} = corrosion current density in $\mu\text{A cm}^{-2}$, 3270 is a constant which defines the unit for the corrosion rate, EW = equivalent weight of corroding material and d = density of corroding material in g cm^{-3} [23].

$$\text{IE}(\%) = \frac{i_{\text{corr}} - i_{\text{corr}(\text{inh})}}{i_{\text{corr}}} \times 100 \quad (2)$$

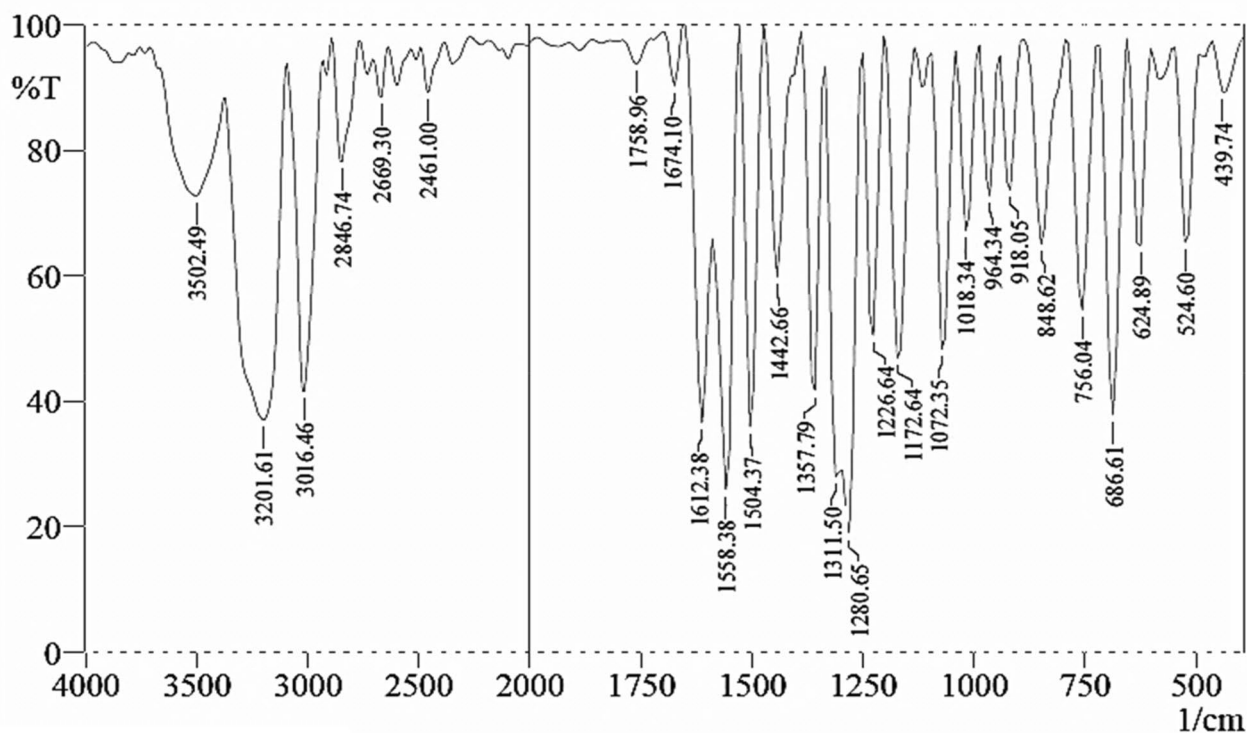
where, i_{corr} and $i_{\text{corr}(\text{inh})}$ signify the corrosion current density in the absence and presence of inhibitors, respectively.

The i_{corr} and CR values in the absence of HBH increased with rise in the temperature. This may be due to increase in the conductance of medium. Whereas as the addition of inhibitor resulted in decrease in both i_{corr} and CR which in turn increases the %IE. This can be due to the adsorption or film formation of the HBH molecules on to the surface of the specimen and thereby blocking sites on the metal surface [24]. 4. The Tafel slope shows the variation in electrode potential if the current flowing in it varies by one order of magnitude. Thus, if the slope (mV decade^{-1}) is lower means less over-potential is required to get high current. That is, application of small-positive potential can cause the reaction to go to a greater extent. In the present case the anodic (β_a) and cathodic (β_c) slope values do not vary much with addition of HBH. This suggests that there is no change in the mechanism of corrosion both in the absence and presence of inhibitor [25].

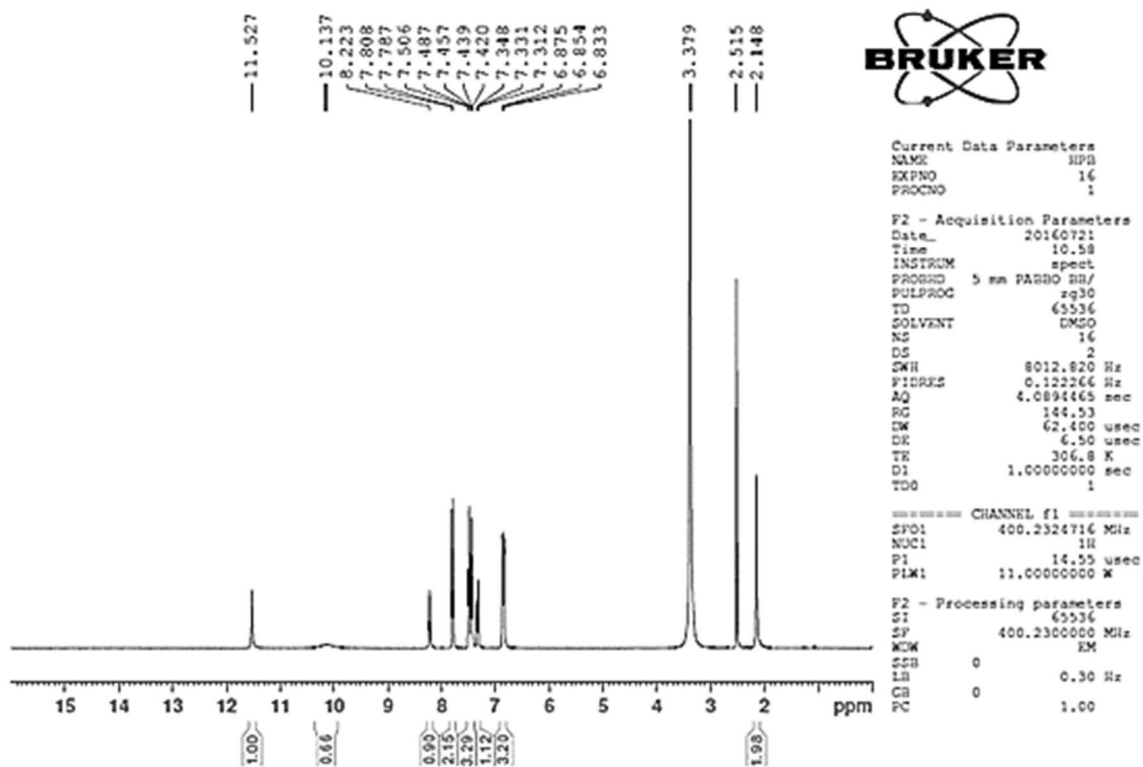
3.3 Electrochemical Impedance Spectroscopy (EIS) Studies

EIS is used to study the corrosion behaviour at the metal-solution interface. Nyquist plots for the corrosion inhibition of Al-CM at different concentrations of HBH at 313 K are given in Fig. 3. The Nyquist plots of Al-CM consist of high-frequency (HF) capacitive loop and intermediate frequency (IF) inductive loop. Shape of these impedance plots agree very well with those reported in the literature [25].

The capacitive loop formed at higher frequency range corresponds to the oxidation of Al-CM at $\text{M}^+/\text{oxide}/\text{solution}$ interface. Al^{1+} will be oxidized to Al^{3+} during the corrosion process which is because of the transport of Al^{1+} from



(a) FTIR spectrum of HBH



(b) ¹H NMR spectrum of HBH

Fig. 1 FTIR spectrum of HBH

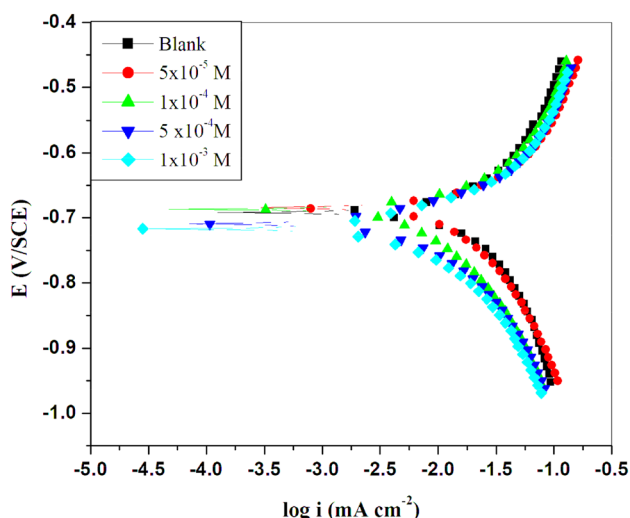


Fig. 2 PDP curves for the corrosion behaviour Al-CM in 0.5 M HCl at 313 K in absence and presence of HBH

M⁺/oxide interface through oxide/electrolyte interface and also O²⁻ and OH⁻ ions are formed at oxide/solution interface. The formation of single capacitive loops in the Fig. 3 indicate that it is undergoing all the above three processes which might be either due to the overlapping of loops during the corrosion process or domination of one process over the other. The formation of passivating oxide film on the metal surface attributes to the capacitive loop in high-frequency region. The resistance offered by the metal towards the corrosion process is increased with increase in the diameter of the semicircle [26]. At lower frequency (LF) the origin of the inductive loop has often been attributed to surface or bulk relaxation of species in the oxide layer. The LF inductive

loop may be related to the relaxation process obtained by adsorption and incorporation of chloride ions, oxide ion and charged intermediates on and into the oxide film. The inductive loop is also attributed to anodic adsorbed intermediates controlling the anodic process [27, 28]. The capacitive loops of the Nyquist plots are comparatively depressed due to the inhomogeneity, roughness of the working electrode surface, deposition of the corrosion product or adsorption of the inhibitor molecules [29].

To carry out mathematical analysis of the EIS technique, the Nyquist plots were simulated with the equivalent circuit. This circuit constitute five elements namely resistance offered by the solution (R_s), resistance offered by charge transfer process (R_{ct}), inductive element (L) and inductive resistance (R_l). It also consists of CPE (Constant Phase Element, Q), which is parallel to resistors and inductive element shown in the Fig. 4. Similar circuits were reported by other researchers for AL-CM in acid medium [17, 25]. The polarization resistance (R_p) from the above circuit can be evaluated using Eq. (3).

$$R_p = \frac{R_{ct} \times R_L}{R_{ct} + R_L} \times 100 \tag{3}$$

During the circuit fitment the real capacitance (C_{dl}) is replaced by constant phase element CPE (Q), because the impedance plots for composite materials are depressed semicircles. The depression in the semicircle is attributed for frequency dispersion that occurs during the impedance analysis because of surface inhomogeneity/surface roughness [29]. The CPE impedance (Z_{CPE}) is calculated using the following equation,

Table 2 PDP results for the corrosion of Al-CM in 0.5 M HCl in the absence and presence of HBH at different temperatures

Temp (K)	Conc. Of HBH (M)	E_{corr} (mV SCE ⁻¹)	$-\beta_c$ (mV dec ⁻¹)	β_a (mV dec ⁻¹)	i_{corr} (mA cm ⁻²)	CR (mpy)	% IE
303	0	-671	585	507	0.0134	4863	-
	5×10^{-5}	-680	680	599	0.0047	2026	64.7
	1×10^{-4}	-687	707	696	0.0030	1304	77.3
	5×10^{-4}	-691	782	781	0.0024	1039	81.9
	1×10^{-3}	-727	867	1520	0.0019	818.7	85.7
313	0	-675	456	484	0.0174	7495	-
	5×10^{-5}	-682	615	549	0.0086	3707	50.5
	1×10^{-4}	-689	662	583	0.0055	2362	68.4
	5×10^{-4}	-703	681	726	0.0032	1393	81.4
	1×10^{-3}	-724	687	1100	0.0029	1253	83.2
323	0	-692	401	457	0.0255	10,960	-
	5×10^{-5}	-685	509	499	0.0155	6650	39.0
	1×10^{-4}	-687	586	515	0.0119	5130	53.2
	5×10^{-4}	-709	631	681	0.0058	2491	77.2
	1×10^{-3}	-717	635	769	0.0050	2146	80.4

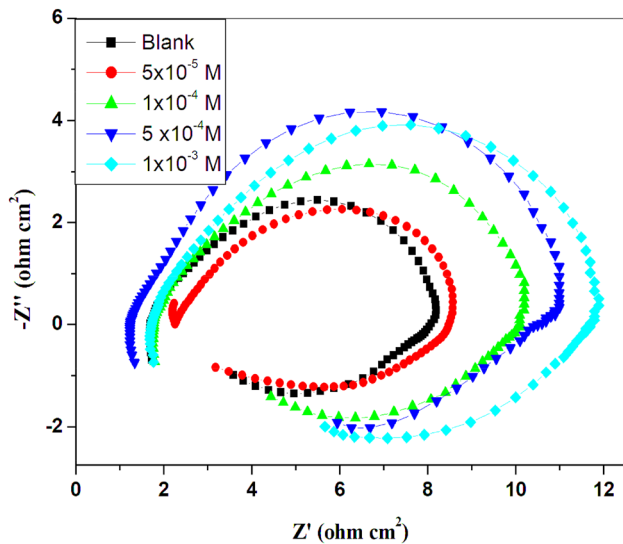


Fig. 3 Nyquist curves for the corrosion behaviour Al-CM in 0.5 M HCl at 313 K in absence and presence of HBH

$$Z_{CPE} = Q^{-1}(i w_{max})^{-n} \tag{4}$$

where Q is the proportionality coefficient, w_{max} is the angular frequency, i is the imaginary number and n is the exponent related to the phase shift. The values of phase shift (n) lies between 0 and 1 ($0 \leq n \leq 1$) [30]. This is related to the deviation of CPE from the ideal capacitive behaviour. The modification in the capacitance to its real value is calculated using the relation 5.

$$C_{dl} = \frac{1}{2\pi R_p f_{max}} \tag{5}$$

where C_{dl} is the double-layer capacitance, R_p is the polarization resistance and f_{max} is the frequency in Nyquist plot at which the imaginary part of the impedance is maximum [30].

The % IE can be obtained using the Eq. 6 [31].

$$\%IE = \frac{R_{p(inh)} - R_p}{R_{p(inh)}} \times 100 \tag{6}$$

where R_p and $R_{p(inh)}$ are the polarization resistance for the blank and in the presence of HBH. Table 3 represents the results of EIS studies for HBH. It is clear from the Table that, polarisation resistance (R_p) values of Al-CM increases with the addition of HBH and the increase is consistent with rise in the concentrations of the HBH. This indicates the resistance against the flow of electrons due to the film formation of inhibitor on the metal surface [31]. The capacitance of electrical double layer (C_{dl}) decreased with increase in inhibitor concentrations. This may be due to increased thickness of the electrical double layer at metal-solution interface. There will be formation of electrical double layer at the metal surface and solution which is equivalent to an electrical capacitor. Further, the decrease in C_{dl} values may be due to the replacement of initially adsorbed water molecules on the metal surface by the HBH molecules [32].

Fig. 4 Equivalent circuit used to fit the experimental EIS data obtained for the corrosion behaviour of Al-CM in the presence of HBH

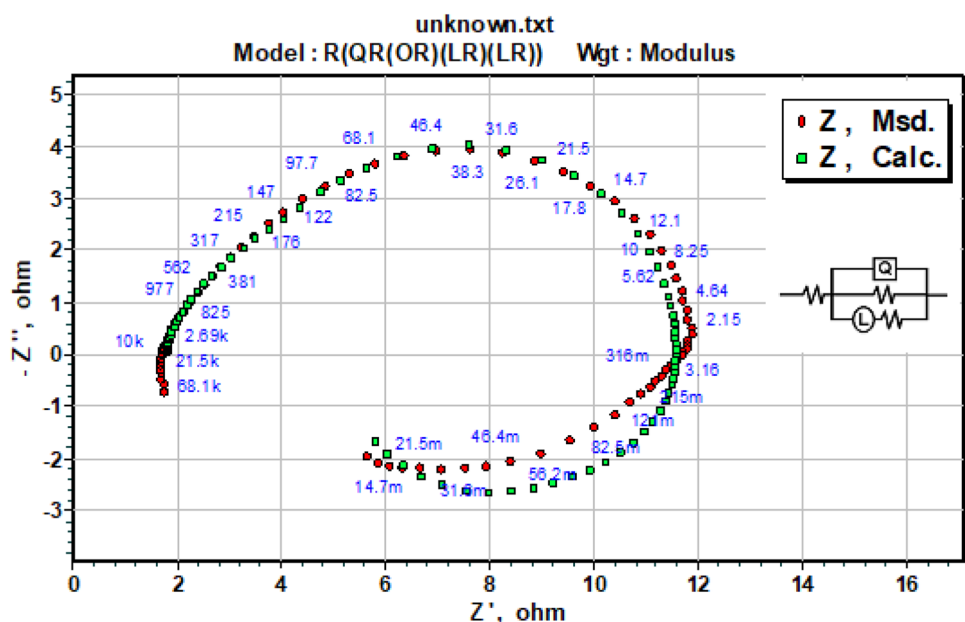


Table 3 EIS results for the corrosion of Al-CM in 0.5 M HCl in the absence and presence of inhibitor at different temperatures

Temp (K)	Conc of HBH (M)	R_p (Ω cm ²)	C_{dl} (μ F cm ⁻²)	n	% IE
303	0	4.100	8.04	0.780	–
	5×10^{-5}	10.27	4.12	0.775	60.5
	1×10^{-4}	16.24	2.44	0.784	75.0
	5×10^{-4}	20.82	1.13	0.797	80.5
	1×10^{-3}	24.02	0.70	0.808	83.1
313	0	1.700	40.0	0.785	–
	5×10^{-5}	3.547	18.4	0.766	52.8
	1×10^{-4}	4.852	10.3	0.78	65.5
	5×10^{-4}	7.822	4.90	0.789	78.6
	1×10^{-3}	8.455	3.20	0.804	80.2
323	0	0.800	95.8	0.775	–
	5×10^{-5}	1.489	70.4	0.754	43.4
	1×10^{-4}	1.960	31.1	0.765	57.0
	5×10^{-4}	3.267	16.2	0.782	74.2
	1×10^{-3}	3.587	9.90	0.836	76.5

3.4 Evaluation of Kinetic Parameters

The study of effect of temperature enables calculations of kinetic factors such as activation energy (E_a), enthalpy (ΔH^\ddagger) and entropy (ΔS^\ddagger) of activation. These parameters are useful in determining the mode of adsorption of HBH molecules on to the specimen surface. The % IE of HBH is found to be decreased with increase in temperature. This could be due to possible desorption of adsorbed HBH molecules from the Al-CM surface. Further the adsorption of HBH on the specimen surface decreases at higher temperature due to the higher rate of hydrogen gas evolution [33]. This type of behaviour suggests physisorption of the HBH molecules on Al-CM. Using Arrhenius Eq. (7) the energy of activation (E_a) can be calculated [34],

$$\ln(\text{CR}) = B - \frac{E_a}{RT} \tag{7}$$

where B is an Arrhenius constant which depends on the metal type, and R is the universal gas constant ($8.314 \text{ J K}^{-1} \text{ mol}^{-1}$), CR is corrosion rate, E_a is energy of activation, T is absolute temperature. Figure 5 shows the Arrhenius plot of $\ln \text{CR}$ vs $1/T$ for the Al-CM in different concentrations of HBH in 0.5 M HCl. E_a values are evaluated from the slope of straight line (slope = E_a/R) obtained.

The transition state equation [35] is used to compute the enthalpy (ΔH^\ddagger) and entropy (ΔS^\ddagger) of activation for the corrosion of Al-CM in the absence and presence of HBH.

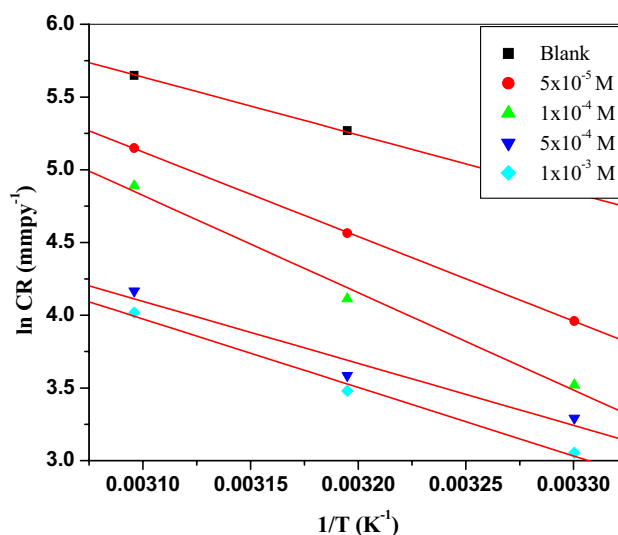


Fig. 5 Arrhenius plot for the corrosion of Al-CM in 0.5 M HCl containing different concentrations of HBH

$$\text{CR} = \frac{RT}{Nh} \exp\left(\frac{\Delta S^\ddagger}{RT}\right) \exp\left(\frac{-\Delta H^\ddagger}{RT}\right) \tag{8}$$

where h is Plank’s constant ($6.626 \times 10^{-34} \text{ J s}$), and N is Avagadro’s number ($6.023 \times 10^{23} \text{ mol}^{-1}$). Figure 6 is the plot of $\ln(\text{CR}/T)$ vs $1/T$ for Al-CM in 0.5 M HCl in various concentration of HBH. Change in values of ΔH^\ddagger an ΔS^\ddagger were calculated from the slope and intercept, respectively, of the plot. Table 4 indicates the activation parameter values for the Al-CM in 0.5 M HCl using various concentration of HBH.

From Table 4, it is evident that E_a value is higher in the presence of HBH than in case of uninhibited. This is because

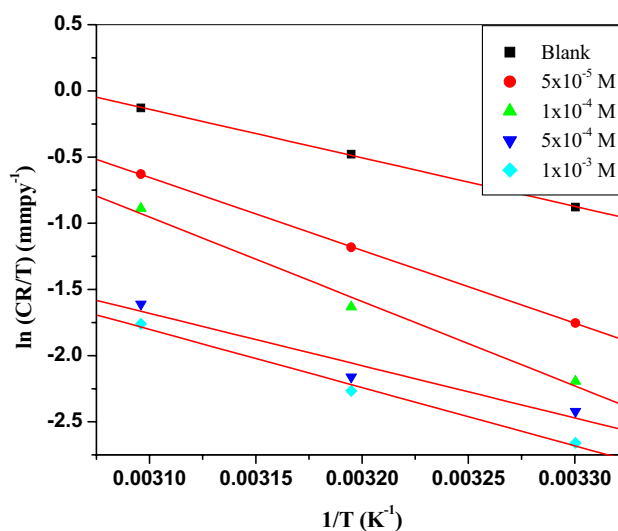


Fig. 6 Plots of $\ln(\text{CR}/T)$ vs $1/T$ for the corrosion of Al-CM in 0.5 M HCl containing different concentrations of HBH

Table 4 Activation parameters obtained for the corrosion of Al-CM in 0.5 M HCl acid containing various concentrations of HBH

Conc. of HBH (M)	E_a (kJ mol ⁻¹)	ΔH^\ddagger (kJ mol ⁻¹)	ΔS^\ddagger (J mol ⁻¹ K ⁻¹)
0	33.07	30.47	-104.2
5×10^{-5}	48.34	45.74	-61.15
1×10^{-4}	55.62	53.02	-41.07
5×10^{-4}	60.38	57.78	-26.56
1×10^{-3}	64.08	61.47	-16.09

of increase in the energy barrier for the corrosion in the presence of HBH. The physical adsorption of the inhibitor molecules on the metal surface can be ascertained due to the increase in the E_a value with increase in the HBH concentration [36]. During corrosion reaction the charge transfer on the surface of the composite will be blocked by the physical adsorption of the HBH molecules which is indicated by an increase in the E_a value [37]. The negative value of ΔS^\ddagger indicates that the randomness is decreased on going from reactants towards the activated complex.

3.5 Mechanism of Adsorption

The adsorption isotherm furnishes basic details about the interaction between inhibitor and the metal surface which helps to determine the corrosion inhibition mechanism by appropriately fitting the experimental results to different adsorption isotherms models. The fraction of surface covered (θ) for different concentration of the HBH was determined. In the present study, Langmuir’s adsorption isotherm (Eq. 9) showed the best correlation between the isotherm function and the results which were obtained experimentally [38].

$$\frac{C_{inh}}{\theta} = \frac{1}{K} + C_{inh} \tag{9}$$

where θ is the surface coverage, C is the concentration of the HBH, K is the equilibrium constant (L mol⁻¹). The plot of C_{inh}/θ versus C_{inh} is a straight line with an intercept of $1/K$. The Langmuir adsorption isotherm for the adsorption of HBH on Al-CM is depicted in Fig. 7. The straight lines with the linear correlation coefficient (R^2) values close to unity, which suggests that the adsorption of HBH in 0.5 M HCl medium on Al-CM surface obeys the Langmuir adsorption isotherm model [39]. The slope values of these lines are range from 1.15–1.17 in the temperature range of 30–50 °C, respectively, suggesting that the adsorbed molecules form monolayer on the Al-CM surface and there is no interaction among the adsorbed inhibitor molecules.

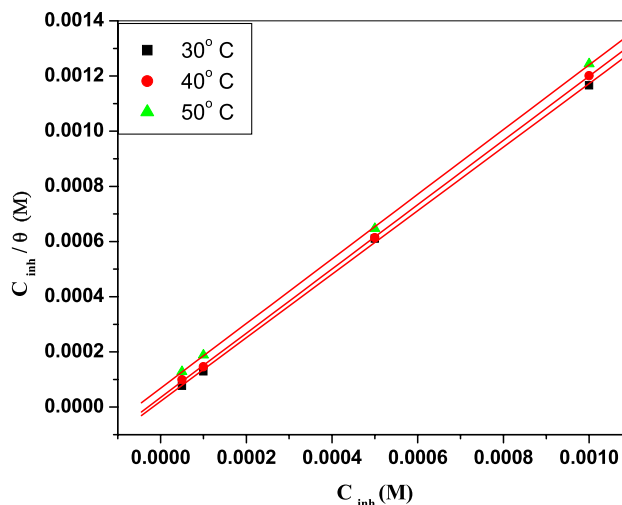


Fig. 7 Langmuir’s adsorption isotherm for Al-CM in 0.5 M HCl containing various concentrations of HBH at different temperature

The standard-free energy of adsorption (ΔG_{ads}°) of the HBH on the metal surface, is related to adsorption/desorption constant K by the Eq. (10).

$$K = \frac{1}{55.5} \exp\left(\frac{-\Delta G_{ads}^\circ}{RT}\right) \tag{10}$$

where, K is the equilibrium constant, T is absolute temperature, R is the universal gas constant and 55.5 is the concentration of water in solution in mol/dm³ [40].

The plot of ΔG_{ads}° Vs T which gives a straight line is shown in Fig. 8. The intercept and slope values are used to calculate the values of standard enthalpy (ΔH_{ads}°) and standard entropy (ΔS_{ads}°) of adsorption, respectively, using the Eq. (11) and the calculated adsorption parameters for the corrosion of AL-CM in 0.5 M HCl in the presence of HBH are recorded in Table 5.

$$\Delta G_{ads}^\circ = \Delta H_{ads}^\circ - T\Delta S_{ads}^\circ \tag{11}$$

The spontaneous adsorption and stability of the adsorbed HBH on the Al-CM surface was quantified by the negative values of ΔG_{ads}° . Generally, if the measure of ΔG_{ads}° is around -20 kJ mol⁻¹ or less negative, then it indicates physisorption of inhibitor molecule, while those with around -40 kJ mol⁻¹ or more negative, shows chemisorption of the inhibitor molecules on the metal surface [41]. The ΔG_{ads}° values for HBH were shown to lie in between -20 and -40 kJ mol⁻¹ which suggests mixed adsorption with predominant physisorption of HBH on Al-CM. The negative value of ΔH_{ads}° specifies the exothermic process due to the physisorption of HBH and the negative value of ΔS_{ads}° indicates

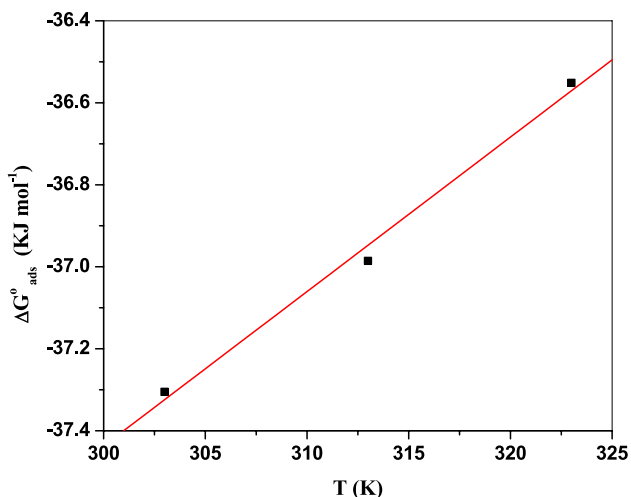


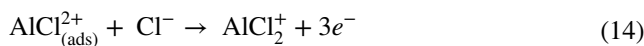
Fig. 8 Plot of ΔG_{ads}° vs. T for Al-CM in the presence of HBH in 0.5 M HCl

the decrease in dis-orderness from the reactant to the adsorbed species [42].

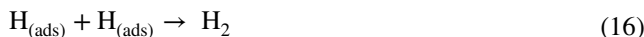
3.6 Mechanism of Corrosion Inhibition

Aluminum composites are comprised of aluminum matrix and ceramic SiC (Silicon Carbide) particulates. In presence of SiC particulates, the continuous oxide layer of aluminum gets broken down. The discontinuous oxide film on aluminum surface increases the corrosion rate. However, aluminum with lower standard electrode potential of -1.66 V acts as anode and undergo oxidation readily whereas SiC particulates being semi-conductors behaves as cathodic site. These cathodic sites favour hydrogen reduction. Formation of micro-galvanic cell is also quite probable in presence of conducting medium [43].

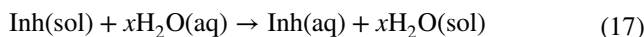
The protective oxide layer formed on aluminum gets depleted in the presence of HCl medium leading to corrosion. The following reactions occur as the potential of aluminum is -1.66 V.



The cathodic reduction reaction in acid medium is,



The process of corrosion inhibition is a surface phenomenon. Several factors like number of active centres on the metal surface, charge density, size of inhibitor and metal-inhibitor interactions play a very important role in protecting the metal against corrosion [44]. In case of HBH, the hetero atoms such as oxygen and nitrogen, unsaturated double bonds and Π electrons of the benzene ring are considered as some of the adsorption centres. The adsorption of the HBH onto the AL-CM in aqueous solution is regarded as aqua-substitution between the inhibitor molecule in aqueous phase [Inh(aq)] and water at the metal surface [H₂O(sol)].



In the presence of acidic medium HBH molecules get protonated and adsorbed to $AlCl^{-}(ads)$ and decreases the further oxidation reaction. The charge on the Al-CM decides the process of adsorption in an aggressive environment. Metal usually surrounded by the positively charged ions in the aggressive environment. This is because of the electric field that emerges at the interface on immersion into the electrolyte.

The charge on the metal depends upon the value of the pH_{Zch} , which is defined as the pH at the point of zero charge potential. Since the pH_{Zch} value for aluminium is 9.1, thus it acquires positive charge in the vicinity of an acidic environment. The positively charge metal ions repulse the adsorption of protonated inhibitor molecule and facilitate the adsorption of negatively charged chloride ions. The negatively charged metal surface attracts the protonated HBH molecule from the corrosive environment through electrostatic interaction and forms a protective physical barrier on the metal surface. The protective layer isolates the metal from direct contact with the aggressive environment and reduces the material loss [45]. The schematic representation for the adsorption of HBH on Al-CM through electrostatic interaction is shown in Fig. 9.

Table 5 Adsorption parameters for the corrosion of AL-CM in 0.5 M HCl containing various concentrations of HBH at different temperature

Temp (K)	K_{ads} (M^{-1})	Slope	R^2	ΔG_{ads}° ($kJ\ mol^{-1}$)	ΔH_{ads}° ($kJ\ mol^{-1}$)	ΔS_{ads}° ($J\ mol^{-1}\ K^{-1}$)
303	48,258.8	1.15	0.999	-37.28		
313	28,946.6	1.16	0.999	-37.18	-48.74	-0.037
323	14,687.1	1.17	0.999	-36.56		

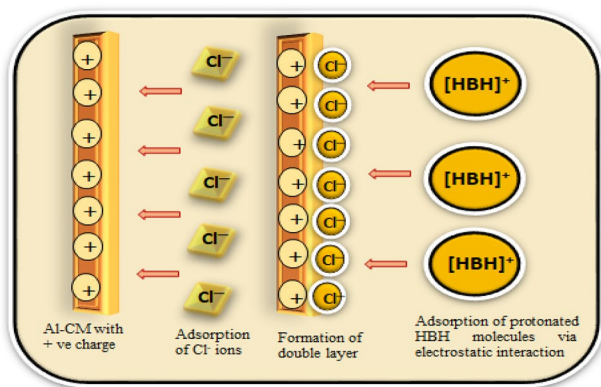


Fig. 9 Schematic representation of physical adsorption of the inhibitor molecule on the metal surface

Further, the inhibition efficiency of HBH is compared with the similar type of inhibitor compounds as reported in the work [17], the hydrazide derivative, namely 4-(*N,N*-dimethyl amino) benzaldehyde thiosemicabazone on 6061 Al-15 vol. pct. Sic(p) composite in a mixture of 1 M hydrochloric and 0.5 M sulphuric acid medium. It showed inhibition efficiency in the range of 50% to 79% at higher inhibitor concentration (1000 ppm) at different temperatures in 1 M HCl + 0.5 M H₂SO₄, whereas HBH showed higher inhibition efficiency in the 80 to 85% at much lower concentration (~200 ppm).

3.7 Theoretical Studies

Quantum chemical calculations were done to understand the structure activity relationship between the molecular structure of HBH and its inhibition efficiency. Generally, corrosion mitigation ability of organic compounds mostly depends upon the electron donating tendency as well as on the nature of its interaction with the surface of the metal [1, 46]. The validation of these effects can be done using DFT study. The DFT calculations points out the electron

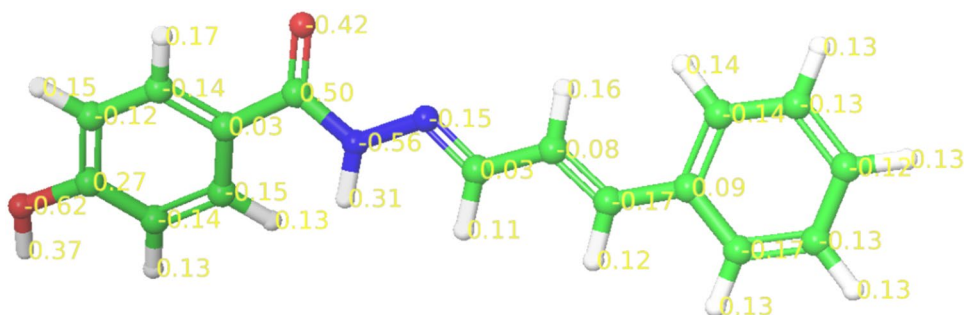
donating and proton accepting sites in the molecules, frontier molecular (HOMO and LUMO) orbital energies, the energy gap between them HOMO and LUMO and the Mullikan's charges present on the molecule. Mullikan charges are widely used to analyse the possible adsorption sites in the inhibitor molecule and also the electron donor–acceptor relation between inhibitor molecules and metal surface. Generally, the hetero-atoms with more negative Mullikan charge are considered to be the most active site for the donor–acceptor relation with the metal surface [47]. The Mullikan charges on the different atoms of HBH is shown in Fig. 10. The more negative charges are noticed on oxygen atoms of OH (−0.62) groups and on the nitrogen (−0.56) atoms. These negative centres can be the adsorption sites for the inhibitor molecules which effectively mitigate the corrosion of Al-CM in acid medium [48].

The optimized structures of the neutral and protonated forms of HBH is depicted in Fig. 11a and b, respectively. The protonated forms were considered alongside the neutral molecules as HBH can undergo protonation in the presence of HCl medium. The optimized structures are supposed to be the most stable ground state geometries of the HBH molecules. Both the neutral and protonated molecule of HBH have planar geometries. These planar molecules show a tendency to aid maximum interactions of the atoms with the metal surface. The co-planarity of the hetero-atoms and the π -electron systems in the inhibitor molecule is accountable for the higher inhibition efficiencies exhibited by the HBH.

The highest occupied molecular orbital (HOMO) and lowest occupied molecular orbitals (LUMO) for neutral and protonated forms of HBH molecules are given in Fig. 12a and b, respectively. Accordingly, some of the studied quantum chemical parameters for neutral and protonated HBH are listed in Table 6.

Generally, the electron density is more localized on hetero atoms of the inhibitor molecule for both HOMO and LUMO. E_{HOMO} may be attributed to the ability to transfer electrons by donation to a definite centre with low empty molecular orbital energy of the molecule that can accept

Fig. 10 Mullikan charges on the different atoms of HBH molecule



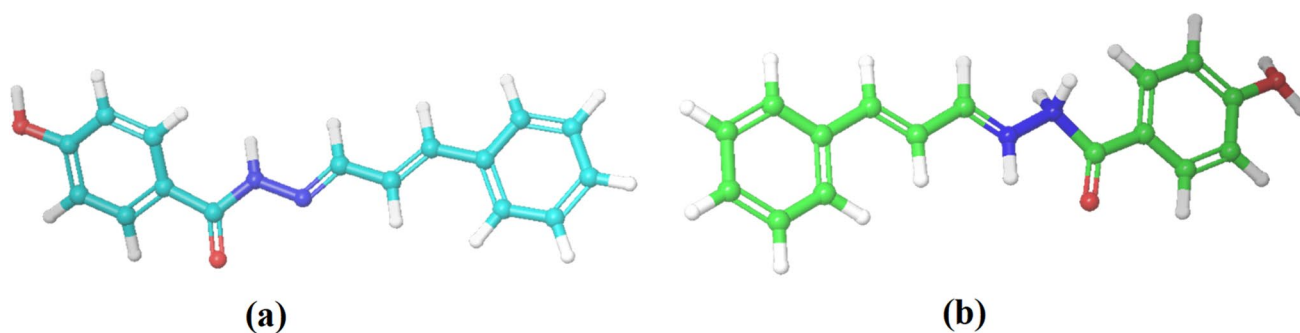


Fig. 11 Optimized structures of **a** neutral HBH and **b** Protonated form of HBH

Fig. 12 HOMO and LUMO structure for **a** neutral HBH and **b** protonated form of HBH

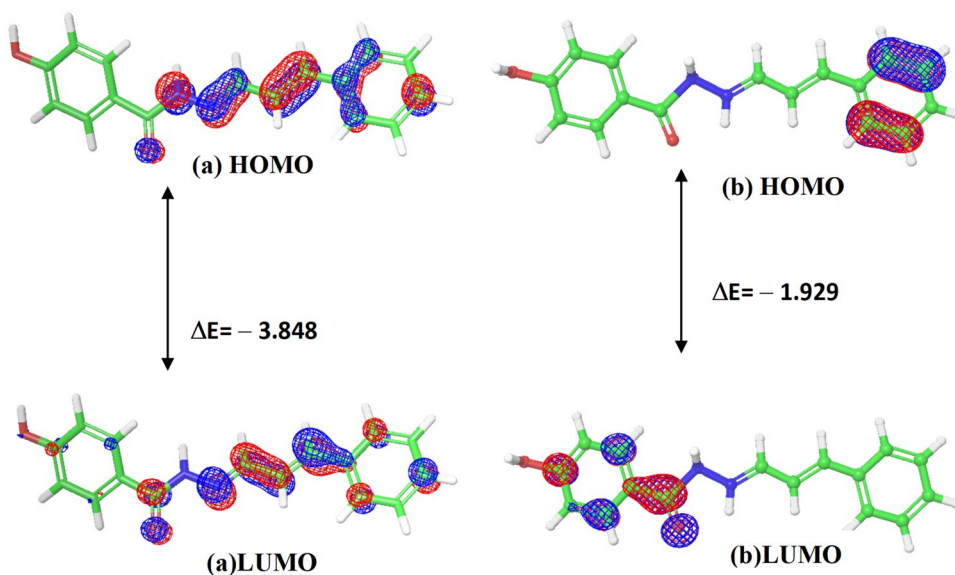


Table 6 Quantum chemical parameters for neutral and protonated HBH

Inhibitor	E_{HOMO} (eV)	E_{LUMO} (eV)	ΔE (eV)	η	σ (eV)	ΔN
Neutral HBH	-5.6962	-1.8474	-3.848	1.924	0.519	0.080
Protonated HBH	-14.748	-12.819	-1.929	0.969	1.031	-5.004

these charge. The added inhibitor can also capture the charge from the metal *d*-orbital formation of a feedback bond. This type of bonds depends mainly on E_{LUMO} values, which ensure that the acceptance of electrons from the metal d orbital [49, 50]. The results in Table 6 indicate that the protonated HBH molecules show a remarkable increase in E_{HOMO} value compared to neutral HBH molecule pointing out an increase in the electron-donating tendency. Similarly, the lower E_{LUMO} values of protonated HBH shows a greater tendency of accepting the electrons with respect to neutral HBH molecules. The other essential parameter is the energy gap or separation energy (ΔE), (the difference between E_{HOMO} and E_{LUMO}). The lower value of ΔE suggest stronger adsorption activity

of inhibitor molecule while the chemical reactivity of the inhibitor increases with decrease in ΔE . This facilitates the adsorption of HBH on to the Al-CM [47]. In the present case the ΔE value for the protonated HBH molecules is lower than the neutral molecules indicating the protonated HBH molecules possesses a higher anti-corrosion ability.

As per the acid–base theory the chemical hardness and softness parameters are related to its inhibition characteristics of the molecule. A soft molecule has higher tendency to react whereas a hard molecule has lower tendency. The decrease in the chemical hardness and increase in the softness values for protonated HBH molecules indicate the greater contribution towards corrosion inhibition process [51]. It is observed that the values of ΔN for neutral and

protonated HBH are 0.080 and -5.004 , respectively. This indicates that the protonated form of HBH has electron accepting tendency while neutral HBH has a tendency to donate the electrons to Al-CM surface [52, 53].

3.8 Surface Morphology Studies

3.8.1 Scanning Electron Microscopy (SEM)

The SEM image of the AL-CM in 0.5 M HCl in the absence of HBH is shown in Fig. 13a. The image showed a rough surface with large number of cavities on the surface of specimen. The increase in the roughness of the surface of Al-CM immersed in 0.5 M HCl can be due to the following reasons.

As the Al-CM comes in contact with acid medium, SiC particulates get removed which leads to formation of cavities on the surface. Generally, galvanic type of corrosion takes place between cathodic SiC particles and anodic aluminum matrix [54]. During the fabrication of composite material, SiC reacts with molten Al to form intermetallic compound Al_4C_3 . Al_4C_3 further reacts with acid by forming $AlCl_3$. The Cl^- ions of the medium interact with $AlCl_3$ and forms $AlCl_4$ [55]. When $AlCl_4$ detaches from the matrix, it leads to the formation of pits. Aluminum and aluminum-based alloys are known for their passive and protective nature due to the presence of an oxide layer on their surface. The reinforcement of SiC particulates in to the matrix may rupture the passive film present on the surface leading to the access of the corrosive medium to the underlying material and hence enhances corrosion [56, 57]. The SEM image of AL-CM obtained in

the presence of 0.5 M HCl containing HBH showed smooth surface as shown in Fig. 13b. The smooth surface is obtained by addition of inhibitor which blocks the separation of SiC particulates thus preventing the formation of cavities.

3.8.2 Energy Dispersive X-Ray Spectroscopy (EDX) Analysis

To determine the elemental composition of the metal surface with and without HBH, EDX studies were carried out. The EDX spectra consists of selected regions of SEM images are given in Fig. 14a and b, respectively. The atomic percentage of elements corresponding to uninhibited and inhibited sample is given in Table 7. Oxygen and chlorine % composition increased in uninhibited solution which is an indication of stable oxide layer undergoing dissolution in the corrosive medium and adsorption of Cl^- on to the metal surface. The increase in the % composition of aluminium, carbon and decrease in the oxygen concentration confirms the adsorption of HBH on the metal surface.

3.8.3 Atomic Force Microscopy (AFM)

Figure 15a and b indicates the 3D image of the Al-CM specimen dipped in uninhibited and inhibited 0.5 M HCl solutions, respectively. Table 8 includes the average surface roughness (R_a) values and root mean square (RMS) roughness (R_q) value. The R_a and R_q value of inhibited specimen were lower than the uninhibited suggesting the adsorption or binding of the HBH molecules on to the metal surface [45].

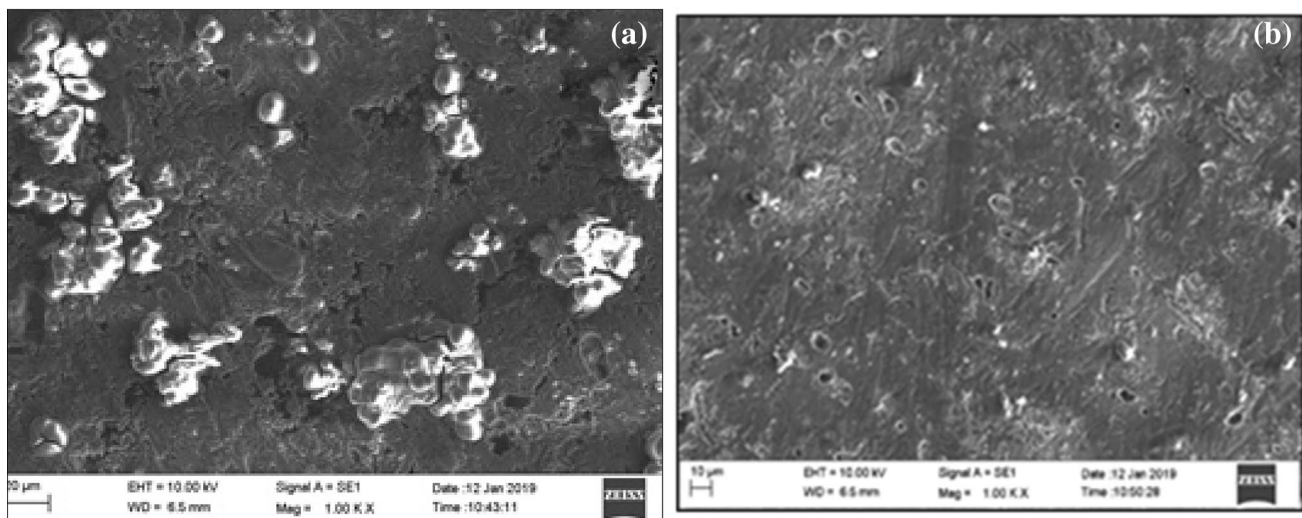


Fig. 13 SEM image of **a** Corroded Al-composite **b** Al-composite immersed in the medium containing inhibitor

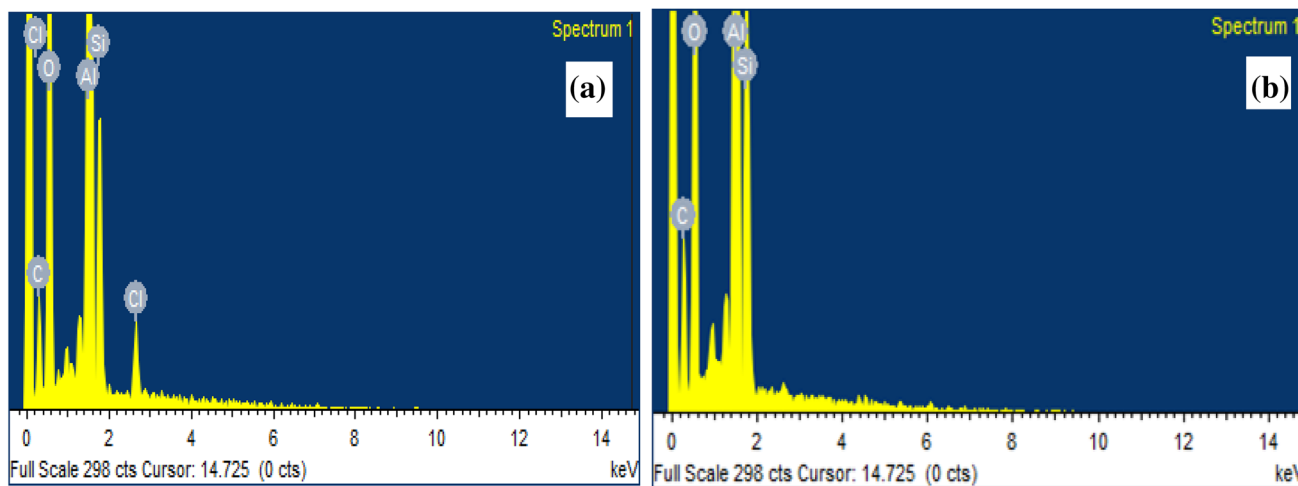


Fig. 14 EDX spectrum of AL-CM **a** exposed to 0.5 M HCl **b** exposed to 0.5 M HCl containing 1×10^{-3} M HBH

Table 7 EDX parameters obtained for the corrosion of Al-CM in the absence and presence of HBH

Samples	% Composition				
	Al	Si	O	Cl	C
Specimen + 0.5 M HCl	33.21	4.29	43.72	1.62	17.17
Specimen + 0.5 M HCl + 1×10^{-3} M HBH	41.43	7.35	29.25	–	21.96

4 Conclusion

Based on the present study carried out of Al-CM in 0.5 M HCl, the following conclusions are drawn.

- HBH can be a potential inhibitor for the corrosion control Al-CM
- Inhibition efficiency of HBH was found to increase with increase in its concentration and decrease with increase in temperature
- HBH functioned as a mixed type of inhibitor and followed Langmuir’s adsorption isotherm
- Mixed adsorption behaviour of HBH is observed with predominant physisorption
- The electronic properties of the inhibitor derived from DFT study clearly explains the inhibition efficiency exhibited by HBH.
- The surface morphological studies such as SEM, EDX and AFM also substantiate the formation of adsorbed layer on the surface of Al-CM

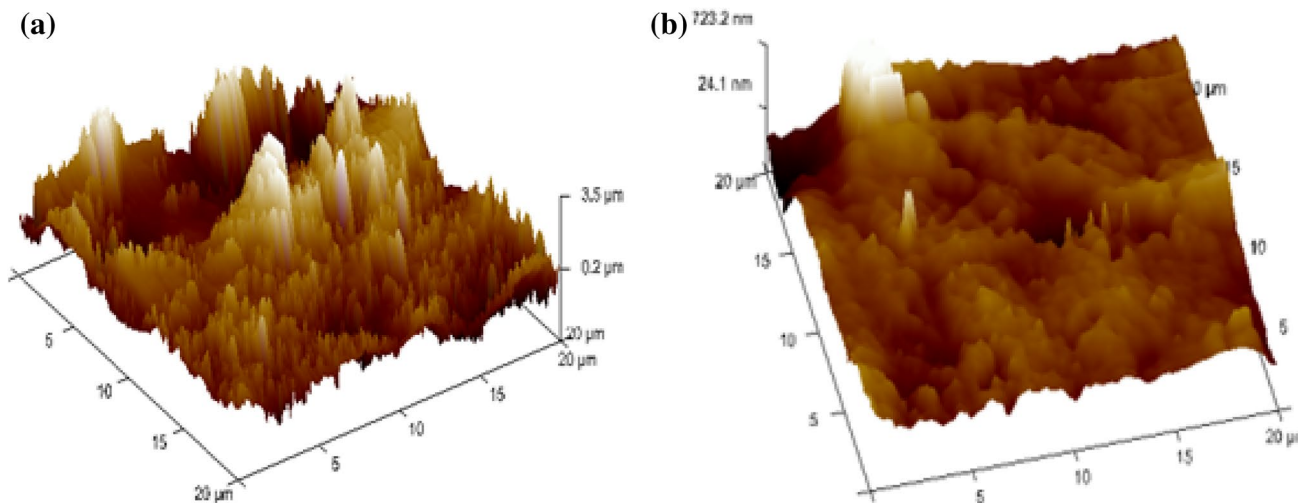


Fig. 15 3D image of AL-CM material **a** immersed in 0.5 M HCl **b** immersed in 0.5 M HCl+ HBH

Table 8 AFM data obtained for the corrosion of Al-CM in the absence and presence of HBH

Samples	R_a (nm)	R_q (nm)
Specimen immersed in 0.5 M HCl	709	914
Specimen + 0.5 M HCl + 1×10^{-3} M HBH	143	198

Compliance with Ethical Standards

Conflict of interest The corresponding author states that there is no conflict of interest.

References

- Goulart CM, Esteves-Souza A, Martinez-Huitle CA, Rodrigues CJF, Maciel MAM, Echevarria A (2013) Experimental and theoretical evaluation of semicarbazones and thiosemicarbazones as organic corrosion inhibitors. *Corros Sci* 67:281–291
- Sharma CP (2004) Engineering materials: properties and applications of metals and alloys. Prentice-Hall of India, New Delhi
- Sayed El, Sharif M (2011) Effects of graphite on the corrosion behavior of aluminum graphite composite in sodium chloride solutions. *Int J Electrochem Sci* 6:1085–1099
- Pardo A, Merino MC, Merino S, Lopez MD, Viejo F, Carboneras M (2003) Influence of reinforcement grade and matrix composition on corrosion resistance of cast aluminium matrix composites (A3xx.x/SiCp) in a humid environment. *Mater Corros* 54:311–317
- Monticelli C, Zucchi F, Brunoro G, Trabanelli G (1997) Corrosion and corrosion inhibition of alumina particulate/aluminium alloys metal matrix composites in neutral chloride solutions. *J Appl Electrochem* 27:325–334
- Merino MC, Merino S, Viejo F, Carboneras M, Arrabal R (2005) Influence of reinforcement proportion and matrix composition on pitting corrosion behaviour of cast aluminium matrix composites (A3xx.x/SiCp). *Corros Sci* 47:1750–1764
- Shahid M (1997) Mechanism of film growth during anodizing of Al-alloy-8090/SiC metal matrix composite in sulphuric acid electrolyte. *J Mater Sci* 32:3775–3781
- Nayak J, Hebbar K (2008) Corrosion inhibition of T-6 treated 6061 Al–SiC(p) composite in hydrochloric acid. *Trans Indian Inst Metals* 61:221–224
- Winkler SL, Ryan MP, Flower HM (2004) Pitting corrosion in cast 7XXX aluminium alloys and fibre reinforced MMCs. *Corros Sci* 46:893–902
- Tang SW, Hu J, Zhao XH (2011) Corrosion behavior of a cerium-based conversion coating on alumina borate whisker-reinforced AA6061 composite pre-treated by hydrogen fluoride. *Corros Sci* 53:2636–2644
- Patel AS, Panchal VA, Mudaliar GV, Shah NK (2013) Impedance spectroscopic study of corrosion inhibition of Al-Pure by organic Schiff base in hydrochloric acid. *J Saud Chem Soc* 17:53–59
- Abdallah M (2004) Antibacterial drugs as corrosion inhibitors for corrosion of aluminium in hydrochloric solution. *Corros Sci* 46:1981–1996
- Branzoi V, Golgovici F, Branzoi F (2003) Aluminium corrosion in hydrochloric acid solutions and the effect of some organic inhibitors. *Mater Chem Phys* 78:122–131
- Kumari P, Shetty P, Rao SA (2017) Electrochemical measurements for the corrosion inhibition of mild steel in 1M hydrochloric acid by using an aromatic hydrazide derivative. *Arab J Chem* 10:653–663
- Kumari P, Shetty P, Rao SA (2015) Corrosion protection properties Of 4-hydroxy-N²-[1E,2E]-3-phenylprop-2-en-1-ylidene] benzohydrazide on mild steel in hydrochloric acid medium. *Pro Met Phy Chem Surf* 15:1034–1042
- Kumari P, Shetty P, Rao SA, Sunil D (2017) Inhibition behaviour of 2-[(2-Methylquinoline-8-yl)Oxy] acetohydrazide on corrosion of mild steel in hydrochloric acid solution. *Trans Indian Inst Met* 70:1139–1150
- Pinto GM, Nayak J, Shetty AN (2011) Corrosion inhibition of 6061 Al–15 vol. pct. SiC(p) composite and its base alloy in a mixture of sulphuric acid and hydrochloric acid by 4-(N, N-dimethyl amino) benzaldehyde thiosemicarbazone. *Mater Chem Phys* 125:628–640
- Lee C, Yang W, Parr RG (1988) Development of the Colle-Salvetti correlation-energy formula into a functional of the electron density. *Phys Rev Condense Mater B* 37:785–789
- Singh P, Ebenso EE, Olasunkanmi LO, Obot IB, Quraishi MA (2016) Electrochemical, theoretical, and surface morphological studies of corrosion inhibition effect of green naphthyridine derivatives on mild steel in hydrochloric acid. *J Phys Chem C* 120:3408–3419
- Verma C, Olasunkanmi LO, Ebenso EE, Quraishi MA, Obot IB (2016) Adsorption behavior of glucosamine-based, pyrimidinefused heterocycles as green corrosion inhibitors for mild steel: experimental and theoretical studies. *J Phys Chem C* 120:11598–11611
- Trowsdale AJ, Noble B, Haris SJ, Gibbins ISR, Thomson GE, Wood G (1996) The influence of silicon carbide reinforcement on the pitting behaviour of aluminium. *Corros Sci* 38:177–191
- Yurt A, Ulutas S, Dal H (2006) Electrochemical and theoretical investigation on the corrosion of aluminium in acidic solution containing some Schiff bases. *Appl Surf Sci* 253:19–925
- Eduok UM, Umoren SA, Udoh AP (2012) Synergistic inhibition effects between leaves and stem extracts of *Sida acuta* and iodide ion for mild steel corrosion in 1 M H₂SO₄ solutions. *Arab J Chem* 5:325–337
- Wang L, Shinohara T, Zhang B (2010) Influence of chloride, sulfate and bicarbonate anions on the corrosion behavior of AZ31 magnesium alloy. *J Alloys Compd* 496:500–507
- Li WH, He Q, Zhang S, Pei S, Hou B (2007) Experimental and theoretical investigation of the adsorption behavior of new triazole derivatives as inhibitors for mild steel corrosion in acid media. *Electrochim Acta* 52:6386–6394
- Charitha BP, Rao P (2017) An ecofriendly approach for corrosion control of 6061 Al-15%(v) SiC(P) composite and its base alloy. *Chin J Chem Eng* 25:363–372
- Aytac A, Ozmen U, Kabasakaloglu M (2005) Investigation of some Schiff bases as acidic corrosion of alloy AA3102. *Mater Chem Phys* 89:176–181
- Abdallah M, Fouda AS, El-Nagar DAM, Alfakeer M, Ghoneim MM (2019) Corrosion inhibition of two aluminium silicon alloys in 0.5 M HCl solution by some azole derivatives using electrochemical techniques. *Surf Eng Appl Electrochem* 55:172–182
- Frers MM, Stefenel C, Mayer CT (2016) AC-impedance measurements on aluminium in chloride containing solutions and below the pitting potential. *J Appl Electrochem* 20:996–999
- Mansfeld F, Lin S, Kim K, Shih H (1987) Pitting and surface modification of SiC/Al. *Corros Sci* 27:997–1000

31. Lebrini M, Robert F, Roos C (2010) Inhibition Effect of alkaloids extract from *annona squamosa* plant on the corrosion of C38 steel in normal hydrochloric acid medium. *Int J Electrochem Sci* 5:1698–1712
32. Xie YJ, Wu J, Che XZ, Chen Y, Huan HW, Deng GJ (2016) Efficient pyrido[1,2-a] benzimidazole formation from 2-aminopyridines and cyclohexanones under metal-free conditions. *Green Chem* 18:667–671
33. Niu L, Yin Y, Guo W, Lu M, Qin R, Chen S (2009) Application of scanning electrochemical microscope in the study of corrosion of metals. *J Mater Sci* 44:4511–4521
34. Larabi L, Harek Y, Benali O, Ghalem S (2005) Hydrazide derivatives as corrosion inhibitors for mild steel in 1 M HCl. *Prog Org Coat* 54:256–262
35. Yahalom J (1972) The significance of the energy of activation for the dissolution reaction of metal in acids. *Corros Sci* 12:867–868
36. Abdel Rehim SS, Magdy AM, Ibrahim KF (1999) 4-Aminoantipyrines an inhibitor of mild steel corrosion in HCl solution. *J Appl Electrochem* 29:593–599
37. Li W, He Q, Zhang S, Pei C, Hou BJ (2008) Some new triazole derivatives as inhibitors for mild steel corrosion in acidic medium. *J Appl Electrochem* 38:289–295
38. Oguzie EE, Njoku VO, Enenebeaku CK, Akalezi CO, Obi C (2008) Effect of hexamethylparosaniline chloride (crystal violet) on mild steel corrosion in acidic media. *Corros Sci* 50:3480–3486
39. Wang X, Yang H, Wang F (2010) A cationic gemini-surfactant as effective inhibitor for mild steel in HCl solutions. *Corros Sci* 52:1268–1276
40. Migahed MA, Mohammed HM, Al-Sabagh AM (2003) Corrosion inhibition of H-11 type carbon steel in 1 M hydrochloric acid solution by N-propyl amino lauryl amide and its ethoxylated derivatives. *Mater Chem Phys* 80:169–175
41. Ashassi-Sorkhabi H, Majidi MR, Seyyedi K (2004) Investigation of inhibition effect of some amino acids against steel corrosion in HCl solution. *Appl Surf Sci* 225:176–185
42. Bentiss F, Traisnel M, Lagrenee M (2001) Influence of 2,5-bis(4-dimethylaminophenyl)-1,3,4-thiadiazole on corrosion inhibition of mild steel in acidic media. *J Appl Electrochem* 31:41–48
43. Martinez S, Stern I (2002) Thermodynamic characterization of metal dissolution and inhibitor adsorption processes in the low carbon steel/mimosa tannin/sulfuric acid system. *Appl Surf Sci* 199:83–89
44. Aylor DM, Moran PJ (1985) Effect of reinforcement on the pitting behavior of aluminum-base metal matrix composites. *J Electrochem Soc* 132:1277–1281
45. Ekpe UJ, Ibok UJ, Ita BI, Offiong OE (1995) Inhibitory action of methyl and phenyl thiosemicarbazone derivatives on the corrosion of mild steel in hydrochloric acid. *Mater Chem Phys* 40:87–93
46. Pinto GM, Nayak J, Shetty AN (2011) Adsorption and inhibitor action of 4-(N, N-dimethylamino) benzaldehyde thiosemicarbazone on 6061 Al/SiC composite and its base alloy in sulfuric acid medium. *Synth React Inorg Org Nano Met Chem* 41:127–140
47. Senhaji O, Taouil R, Skalli MK, Bouachrine M, Hammouti B, Hamidi M (2011) Experimental and theoretical study for corrosion inhibition in normal hydrochloric acid solution by some new phosphonated compounds. *Int J Electrochem Sci* 6:6290–6299
48. Zhang W, Hui-Jing L, Wang M, Li-Juan W, Ai-Han Z, Yan-Chao W (2019) Highly effective inhibition of mild steel corrosion in HCl solution by using pyrido[1,2-a] benzimidazoles. *New J Chem* 43:413–426
49. Ansari K, Quraishi M, Singh A, Ramkumar S, Obote IB (2016) Corrosion inhibition of N80 steel in 15% HCl by pyrazolone derivatives: electrochemical, surface and quantum chemical studies. *RSC Adv* 6:24130–24141
50. Abdallah M, Gad EA, Sobhi M, Fahemi JH, Alfakeer MM (2019) Performance of tramadol drug as a safe inhibitor for aluminium corrosion in 1 M HCl solution and understanding mechanism of inhibition using DFT. *Egypt J Petrol* 28:173–181
51. Zhang K, Xu B, Yang W, Yin X, Liu Y, Chen Y (2015) Halogen-substituted imidazoline derivatives as corrosion inhibitors for mild steel in hydrochloric acid solution. *Corros Sci* 90:284–295
52. Obot IB, Gasem ZM (2014) Theoretical evaluation of corrosion inhibition performance of some pyrazine derivatives. *Corros Sci* 83:359–366
53. Dohare P, Chauhan D, Sorour A, Quraishi M (2017) DFT and experimental studies on the inhibition potentials of expired Tramadol drug on mild steel corrosion in hydrochloric acid. *Mater Discov* 9:30–41
54. Geerlings P, De Proft F, Langenaeker W (2003) Conceptual density functional theory. *Chem Rev* 10:31793–31874
55. Umoren SA, Obot IB, Ebenso EE, Okafor PC, Ogbobe O, Oguzie EE (2006) Gum arabic as a potential corrosion inhibitor for aluminium in alkaline medium and its adsorption characteristics. *Anti-Corros Methods Mater* 53:277–282
56. Carotenuto G, Gallo A, Nicolais L (1994) Degradation of SiC particles in aluminium-based composites. *J Mater Sci* 29:4967–4974
57. Charitha BP, Arunchandran C, Rao P (2017) Enhancement of surface coating characteristics of epoxy resin by dextran: an electrochemical approach. *Ind Eng Chem Res* 56:1137–1147

Publisher's Note Springer Nature remains neutral with regard to jurisdictional claims in published maps and institutional affiliations.